Composites Part B 104 (2016) 44–56

Contents lists available at ScienceDirect

Composites Part B

journal homepage: www.elsevier.com/locate/compositesb

Behaviour of inorganic polymer concrete columns reinforced with basalt FRP bars under eccentric compression: An experimental study

Xiaochun Fan [a], Mingzhong Zhang [b, *]

[a] School of Civil Engineering and Architecture, Wuhan University of Technology, Wuhan, 430070, China
[b] Advanced and Innovative Materials (AIM) Group, Department of Civil, Environmental and Geomatic Engineering, University College London, London, WC1E 6BT, UK

ARTICLE INFO

Article history:
Received 29 March 2016
Received in revised form
11 July 2016
Accepted 17 August 2016
Available online 20 August 2016

Keywords:
Polymer (textile) fibre
Mechanical properties
Strength
Mechanical testing
Geopolymer concrete

ABSTRACT

In this paper, a new composite system for concrete structures, i.e. inorganic polymer concrete column (IPCC) reinforced with basalt FRP bars, which combines the outstanding features of inorganic polymer concrete (IPC) and basalt reinforcement such as good corrosion resistance and fire resistance was proposed. The inorganic polymer binder was made of industrial by-products including fly ash and ground granulated blast-furnace slag, and alkaline activating solution. The mechanical behaviour of short IPCC under eccentric compression was experimentally investigated and compared with control steel-reinforced ordinary Portland cement concrete columns (OPCC). The effect of eccentricity on overall failure mode and load–displacement/strain response of the specimens was studied. Results indicate that the load-carrying capacity of IPCC was approximately 30% lower than that of OPCC, while the ultimate displacements of IPCC were 65% and 15% larger than those of OPCC under large and small eccentricities, respectively. The IPCC specimens had almost similar overall load–displacement/strain response as the OPCC specimens up to the final failure. The ultimate longitudinal strains on the compression face of IPCC under large and small eccentricities were one time and 22% larger than those of OPCC respectively due to the relatively lower strength of IPC than ordinary concrete. In addition, the sine-shaped model can be used for IPCC to predict the lateral deformation along the column length at various load levels until final failure.

1. Introduction

Concrete is the most widely used construction material in the world. Ordinary Portland cement (OPC) has traditionally been used as the binding material in concrete. However, OPC has high embodied energy and the manufacture of OPC accounts for a significant proportion of raw material consumption and contributes nearly 7% of global carbon dioxide emissions [1]. In order to reduce the carbon footprint associated with concrete and enhance the sustainability of concrete infrastructure it is essential to find an alternative binder to OPC for concrete. Inorganic polymers, also called geopolymers, are considered to be one such alternative, which are conventionally produced by synthesizing pozzolanic compounds or alumino-silicate source materials with highly alkaline hydroxide and/or alkaline silicate. Industrial by-products, such as fly ash and ground granulated blast-furnace slag are commonly utilised as the source of inorganic polymer concrete (IPC) because of the low cost and wide availability of these materials. IPC has been found to have many attractive properties compared to OPC concrete, such as little drying shrinkage, low creep, good fire resistance, good resistance to freeze-thaw cycles and acid attack, and can help reduce embodied energy and carbon footprint by up to 80% [2–7].

Corrosion of reinforcing steel is the major cause of deterioration of reinforced and prestressed concrete structures and has been a main concern for many years, as it would lead to cracking, reduction in bond strength, reduction in steel cross section and loss of serviceability. In order to solve steel corrosion problems in concrete, many attempts have been made in recent years including the use of fibre reinforced polymer (FRP) bars as an alternative to steel reinforcement for concrete structures. Aramid FRP (AFRP), carbon FRP (CFRP) and glass FRP (GFRP) are the most commonly used ones. However, AFRP and GFRP bars are very sensitive to alkaline environment within concrete due to the poor alkali resistance of fibres [2] and CFRP bars are still far too expensive for most applications

* Corresponding author.
E-mail address: mingzhong.zhang@ucl.ac.uk (M. Zhang).

http://dx.doi.org/10.1016/j.compositesb.2016.08.020

[8]. Recently, basalt FRP (BFRP) has gathered attention as a replacement for other FRPs because of its cost effectiveness, ease of manufacture, high temperature resistance, freeze-thaw performance, good resistance to corrosion, acids, and vibration and impact loading [9–13]. Moreover, BFRP bars have better durability in alkaline conditions than AFRP and GFRP [11,14]. Due to these outstanding features, there is an increasing application of BFRP bars in civil engineering structures.

During the last few years, many efforts have been made to investigate the mechanical behaviour of BFRP reinforced concrete and steel reinforced inorganic polymer (geopolymer) concrete structural members including beams, columns, slabs and panels, in particular the bond behaviour between concrete and reinforcement, and overall performance. The flexural and shear performance of concrete beams reinforced with BFRP bars has been experimentally studied and presented in Refs. [15–18], which showed that concrete beams reinforced with BFRP bars had higher strengths than control steel-reinforced beams with the same reinforcement ratio, and behaved quite similarly to that of beams reinforced AFRP and GFRP bars. Sumajouw et al. [19] studied the performance of reinforced geopolymer concrete slender columns under axial load and uniaxial bending in single curvature mode, and found that the design provisions contained in the current standards and codes can be used to design reinforced fly ash-based geopolymer concrete columns. Other recent studies [20–25] were carried out to examine the bond strength between basalt rebar and OPC concrete, and steel rebar and geopolymer concrete. It was observed that the overall bond behaviour of OPC concrete with basalt rebar was similar to that of OPC concrete with steel rebar, however, geopolymer concrete with steel rebar had higher bond strength than control OPC concrete. In addition, the existing analytical expressions for bond strength of OPC concrete can be used for predicting bond strength of steel-reinforced geopolymer concrete. These existing findings lead to the idea in this study of combing basalt rebar and IPC (i.e., geopolymer concrete) in a composite system to improve the durability and sustainability of concrete structures. It should be mentioned that the mechanical behaviour of basalt rebar reinforced inorganic polymer concrete structural members including beams and columns has not been extensively addressed to date.

In this work, for the first time, the mechanical behaviour of inorganic polymer concrete columns (IPCC) reinforced with basalt rebar under eccentric compression is investigated and compared with control steel-reinforced ordinary Portland cement concrete columns (OPCC). It extends a recently published work by Fan and Zhang [26] from beams to columns. The mechanical properties of inorganic polymer concrete made of fly ash, ground granulated blast-furnace slag and alkaline activating solution and basalt rebar are measured. The effect of eccentricity on overall failure mode and load–displacement/strain behaviours of the specimens is studied and analysed in detail in order to gain a comprehensive understanding of the failure mechanisms of such new composite system, i.e., IPC columns reinforced with basalt rebar, subjected to eccentric compression loads.

2. Experimental program

2.1. Test specimens

A total of eight short columns were designed and tested: four inorganic polymer concrete columns reinforced with basalt rebar and four ordinary reinforced concrete columns. Each column specimen had a square cross section of 120 mm × 120 mm and an overall height of 900 mm. For each specimen, the test portion had a height of 460 mm and each haunched head had a height of 220 mm. All specimens were reinforced with symmetrically placed longitudinal bars. The transverse reinforcement was provided with rectangular ties Φ 6 @ 100 mm. The thickness of concrete cover was 20 mm. In order to prevent premature failures in haunched heads, extra longitudinal and transverse reinforcement was provided in haunched heads. The specimen layout and reinforcement details for the specimens are shown in Fig. 1.

The main experimental parameters in this study were the types of concrete, types of longitudinal rebar and eccentricity. Two types of concrete including inorganic polymer concrete and ordinary Portland cement concrete; two types of longitudinal reinforcement including basalt rebar and ordinary steel rebar; and two eccentricities of 20 mm and 80 mm were investigated. The specimen design details are summarized in Table 1, where 'B' refers to the basalt rebar and 'O' stands for the ordinary steel rebar.

The specimens were divided into two groups. The first group labelled 'IPCC' consisted of four inorganic polymer concrete columns, and the second group labelled 'OPCC' was composed of four ordinary reinforced concrete columns and served as control specimens. For each group, two specimens were tested under an eccentricity of 80 mm, and the other two were tested under an eccentricity of 20 mm.

2.2. Materials

2.2.1. Concrete

The concrete used in this work was IPC and OPC, respectively. The IPC was made of a mixture of inorganic polymer binder composed of fly ash, ground granulated blast-furnace slag (GGBS) and alkaline activating solution, fine aggregate and coarse aggregate. The chemical compositions of fly ash and GGBS are given in Table 2. The alkaline activating solution was obtained by dissolving solid sodium hydroxide (NaOH) into sodium silicate (Na_2SiO_3) solution with the Na_2SiO_3/NaOH ratio of 1.53. Fifteen series of inorganic polymer binder were prepared and tested in order to determine the optimal composition of the mixture considering both early-age properties and durability, which was presented in detail in previous work [10,26]. The medium-sized sand with fineness modulus of 2.72 was used as fine aggregate. The coarse aggregate was 13 mm nominal size crushed stone. The particle size distributions of fine and coarse aggregates are presented in Tables 3 and 4, respectively.

Table 5 illustrates the mix proportion of IPC and OPC. According to GB/T 50081-2002 [27], uniaxial compressive strength was measured at 3, 7 and 28 days on 100 mm concrete cube and the elastic modulus was measured at 28 days on rectangular concrete prism with dimensions of 150 mm × 150 mm × 300 mm. The time evolution of compressive strength and elastic modulus of concrete are shown in Table 6. A very similar trend in the strength development can be found for IPC and OPC, although the compressive strength of IPC at each curing age was around 80% of that of OPC. The compressive strength at 3 days and 7 days were approximately 48% and 66% of that at 28 days, respectively. The elastic moduli of IPC and OPC were very close.

2.2.2. Reinforcement

According to the manufacturer, the basalt rebar for IPCC (as shown in Fig. 2) has a specified elastic modulus, yield strength and ultimate tensile strength of 50 GPa, 600 MPa and 1000 MPa, respectively. Herein, standard uniaxial tension tests were carried out on five 8-mm-diameter basalt rebars to obtain their stress–strain response, which is shown in Fig. 3. The stress–strain curves show that there exhibits an initial linear elastic region followed by a very small hardening branch until ultimate failure. However, the yielding point was not obvious. The average yield strength of five basalt rebars was approximately 625 MPa. The average tensile

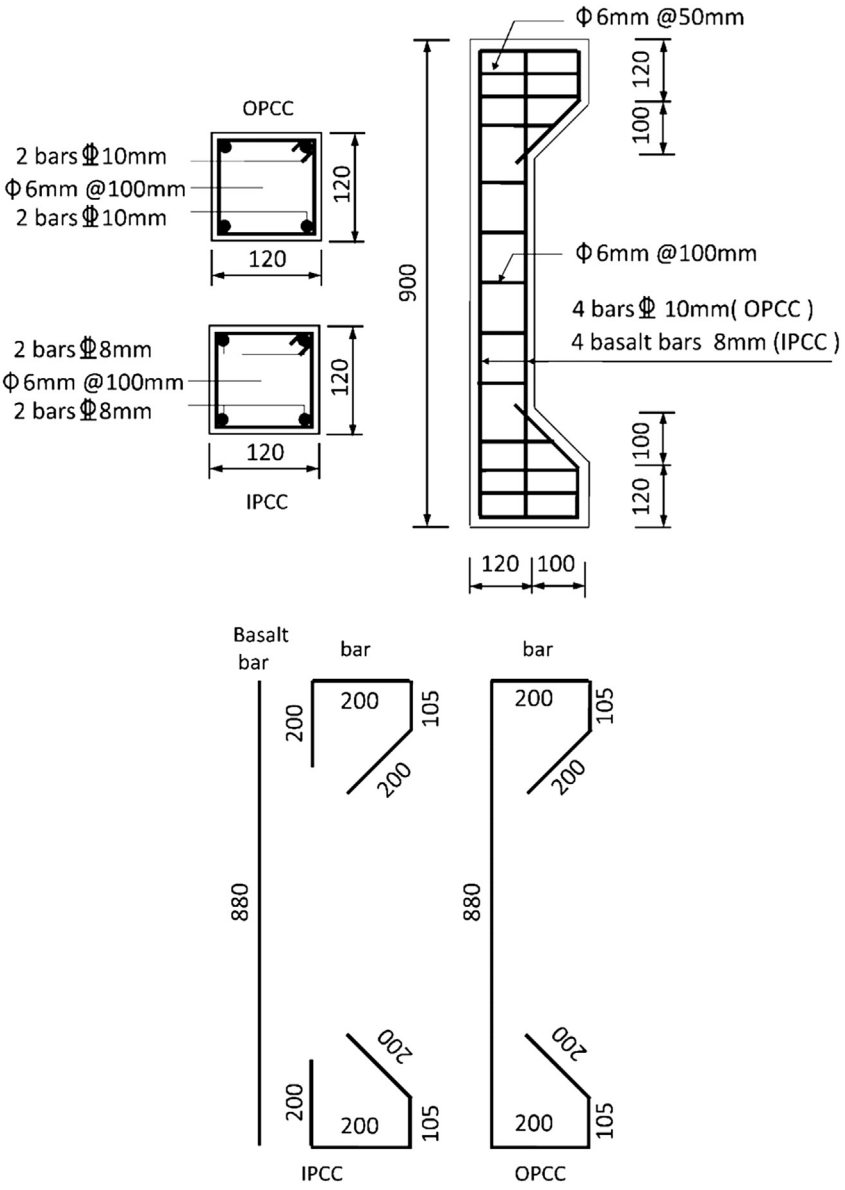

Fig. 1. Specimen layout and reinforcement details for the specimens.

Table 1
Specimen design details.

Specimen	Longitudinal reinforcement	Longitudinal reinforcement ratio (%)	Eccentricity (mm)
IPCC-LE1,2	B4Φ8	1.4	80
IPCC-SE1,2	B4Φ8	1.4	20
OPCC-LE1,2	O4Φ10	2.18	80
OPCC-SE1,2	O4Φ10	2.18	20

strength of them was around 645 MPa. The actual elastic module was found to be 48 GPa. The longitudinal reinforcement used for OPCC was 12-mm-diameter steel rebar (HRB400 type) with yield strength of 360 MPa and ultimate tensile strength of 540 MPa. The transverse reinforcement for specimens were steel rebars (HPB300 type) whose yield strength was 270 MPa.

For the purpose of comparison with the control columns, i.e. OPCC, the diameter of basalt rebar for IPCC should be determined beforehand. In this work, the method of equal-strength substitution was applied to the determination of diameter of basalt rebar. As such, steel rebar is replaced with basalt rebar, while the latter has the same strength, i.e. $d_1^2 f_{y,1} = d_2^2 f_{y,2}$, in which d_1 and d_2 are the diameters of steel and basalt rebars, and $f_{y,1}$ and $f_{y,2}$ represent their nominal yield strength, respectively. The diameter of basalt rebar calculated using the method of equal-strength substitution was 9.1 mm. However, the rebar in 9 mm diameter is not available in the specifications for rebar. Therefore, the 8-mm-diameter basalt rebar was chosen and used for IPCC. It should be noted that this would result in an approximately 30% greater contribution of reinforcement to OPCC than IPCC.

Table 2
Chemical composition of fly ash and ground granulated blast furnace slag (wt %).

Composition	Fly ash	Slag
Calcium oxide, *CaO*	2.99	37.13
Silicon dioxide, SiO_2	51.12	33.20
Aluminium oxide, Al_2O_3	29.53	14.63
Iron oxide, Fe_2O_3	5.57	0.34
Potassium oxide, K_2O	2.38	0.33
Sulphur trioxide, SO_3	1.34	2.97
Magnesium oxide, *MgO*	1.03	9.18
Sodium oxide, Na_2O	0.5	0.32
Barium oxide, *BaO*	0.06	0.36
others	2.42	1.20
Loss of ignition (LOI)	3.06	0.34

Table 3
Particle size distribution of fine aggregates in inorganic polymer concrete.

Sieve size (mm)	Total percentage retained (%)	Total percentage passing (%)
4.75	0	100
2.36	13.74	86.26
1.18	30.36	69.64
0.60	49.50	50.50
0.30	84.34	15.66
0.15	96.98	3.02
0.075	98.98	1.02

Table 4
Particle size distribution of coarse aggregates in inorganic polymer concrete.

Sieve size (mm)	Total percentage retained (%)	Total percentage passing (%)
20.00	0	100
19.00	1.30	98.70
16.00	16.66	83.34
13.20	50.28	49.72
9.50	87.62	12.38
4.75	99.70	0.30

2.3. Specimen preparation

The specimens were cast in a wooden formwork from one batch. The reinforcement was assembled and placed inside the formwork in advance. For inorganic polymer concrete, the fine and coarse aggregates were firstly mixed for 2 min. Subsequently, the inorganic polymer binder was mixed together with aggregates for about 3 min followed by a gradual addition of free water. Afterwards, the concrete was poured into the formwork and compacted adequately using a vibrator to ensure an even dispersion of concrete. After 24 h, the specimens were demoulded and immediately placed in a curing room with a controlled temperature of 22 ± 2 °C and 95 ± 5% relative humidity for 28 days.

2.4. Test setup and loading

The axial load was applied to the columns by a hydraulic actuator according to GB/T 50152-2012 [28]. The lower ends of the specimens were supported on the steel reaction frame, while the upper ends were attached to the stiff plate. Both end supports were designed as hinged connections with prescribed eccentricities. For IPCC specimens under large eccentricity, the increment of load was 6 kN, while for other specimens, i.e., IPCC under small eccentricity and OPCC, the increment of load was 10 kN.

In the experiment, a total of 3 displacement gages (LVDTs) and 24 strain gauges (20 strain gauges for longitudinal reinforcement and 4 for concrete) were used for each specimen. The arrangement of displacement gages and strain gauges is shown in Fig. 4. The load was applied through a 2000 kN hydraulic actuator. The entire test

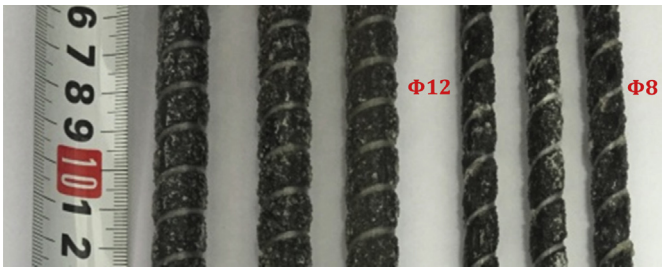

Fig. 2. Basalt FRP bars for inorganic polymer concrete specimens.

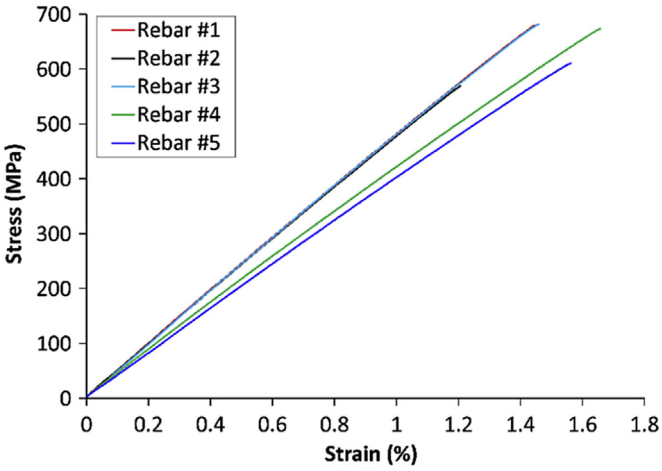

Fig. 3. Stress–strain relationship of basalt FRP bars.

Table 5
Mix proportion of concrete (kg/m^3).

Specimen	Cement	Inorganic polymer binder	Water	Fine aggregate	Coarse aggregate
IPC	–	425	153	615	1262
OPC	340	–	136	633	1298

Table 6
Compressive strength and elastic modulus of concrete.

Specimen	Compressive strength (MPa)			Elastic modulus (GPa)
	3 days	7 days	28 days	28 days
IPC	16.7	23.9	34.9	32.1
OPC	20.5	28.0	42.6	33.0

and measurement was carried out under displacement control. An automatic data acquisition system was utilised to monitor loading. Displacements and strains were monitored by a digital data logger system. The experiments were carried out up to failure of specimens. During the test, force, displacement and strains were obtained and recorded by computer software.

3. Experimental results and discussion

3.1. Failure modes

3.1.1. Large eccentricity

Failure of the ordinary plain concrete columns with large eccentricity (OPCC-LE) and the inorganic polymer concrete columns with large eccentricity (IPCC-LE) is shown in Figs. 5 and 6, respectively. It can be seen that all specimens failed in flexural tension mode by yielding of the longitudinal reinforcement. The development of cracking and crack width were measured for all columns during loading. In order to further demonstrate the cracking patterns of the specimens, OPCC-LE1 and IPCC-LE1 are selected and depicted in Fig. 7. The corresponding load values to crack growth were marked in figures.

For OPCC-LE1, the overall behaviour was typical. At the early stages of loading, the concrete and reinforcement work together to carry the load. The first crack was observed at column mid-height on the tension face at load value of 20 kN. As the load increased, the existing cracks propagated and new cracks formed along the length of column. At a load of around 100 kN, vertical cracks occurred at the lower side of the column. With further increase in load, cracks propagated towards the column compression face. The column was finally crushed at a load of 130 kN. The crack width at the peak load was approximately 2 mm.

The overall behaviour of the inorganic polymer concrete columns under compression with large eccentricity was similar with that of OPCC. The first cracks were noticed on IPCC when the applied load reached about 18 kN, which is a little bit lower than OPCC. This can be attributed to the relatively lower strength of inorganic polymer concrete than ordinary concrete. As the load increased, the noise related to the microcracking of concrete and stretch of basalt rebar became more and more obvious, which indicates the stress redistribution between concrete and rebar within the specimen. The cracks around mid-height were opened extensively. Upon further increasing the applied load, it can be obviously found that cracks on IPCC developed faster and extended deeper towards the compression face of the column in comparison with OPCC. The maximum lateral displacement was almost seen at mid-height section of the specimen. Prior to the failure, there existed more cracks on the upper tension face of the column and the curvature of the specimen became larger. The final failure was characterised by tensile failure of longitudinal basalt rebar and crushing of inorganic polymer concrete in both tension and compression faces near the mid-height of the column. This is different with the cracking pattern of OPCC, in which no cracks occurred on the compression face of the column. This can be ascribed to the fact that the elastic modulus of basalt rebar in IPCC is lower than that of steel rebar in OPCC. Moreover, basalt rebar in IPCC does not have an obvious yield point and its tensile strength is larger than the yield strength of steel rebar in OPCC. For IPCC, the ultimate load capacity was found to be 90 kN, which is approximately 70% of that of OPCC. Additionally, crack width at the peak load for IPCC was around 2.2 mm, which is slightly larger than that for OPCC.

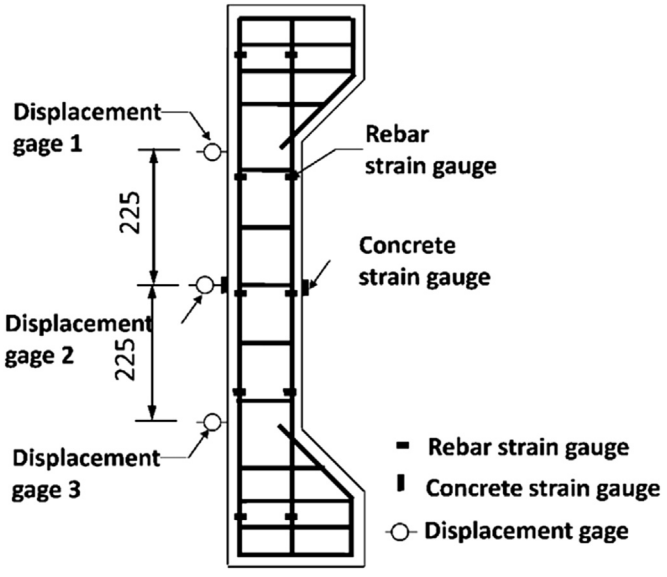

Fig. 4. Arrangement of displacement gages and strain gauges.

3.1.2. Small eccentricity

Figs. 8–10 show the failure of specimens under 20 mm eccentricity. The ordinary plain concrete columns with small eccentricity (OPCC-SE) and the inorganic polymer concrete columns with small eccentricity (IPCC-SE) had similar overall behaviour. Cracking patterns were recorded during the tests for all specimens. OPCC-SE1 and IPCC-SE1 are selected and depicted in Fig. 11 to illustrate the failure modes of columns.

All columns were failed by the concrete crusing on the compression face and ruption of reinforcement. At the early stage of loading, concrete and reinforcement bear the load together, which is similar to that for large eccentricity. Tensile cracks initiated on the tension force at the load values of 150 kN for OPCC and 80 kN for IPCC, respectively. As load increased, more and more short horizontal cracks were produced on the tension face and some relatively long vertical cracks started to occur along the specimen length. This trend became more obvious when the load reached 240 kN for OPCC and 210 kN for IPCC. For OPCC, both the horizontal and vertical cracks propagated fast when the load was close to the ultimate load. For IPCC, the fast crack propagation can be observed when the load was approaching the ultimate load. The load-carrying capacity of OPCC was found to be 380 kN, while the IPCC had a load-carrying capacity of 270 kN, which is approximately 71% of OPCC. This result is almost the same to that observed for the specimens under large eccentricity. It should be noticed that the load capacity for the specimens with short eccentricity was around three times the load capacity for specimens with large eccentricity, which can be attributed to fact that the compressive strength of concrete was larger than its tensile strength. The maximum widths of horizontal cracks were 0.36 mm and 0.2 mm for OPCC and IPCC, respectively. The maximum widths of vertical cracks for them were 0.32 mm and 0.28 mm, respectively.

3.2. Load–displacement curves

3.2.1. Large eccentricity

Fig. 11 presents the load–displacement curves for the specimens of OPCC and IPCC with large eccentricity as shown in Figs. 5 and 6. The lateral displacement was measured from the displacement gage at mid-height of the specimen. Values of loads and mid-height displacements corresponding to the first cracking, the yielding of reinforcement and the final failure of the column are summarized in Table 7. As seen in Fig. 11, OPCC reinforced with steel rebar

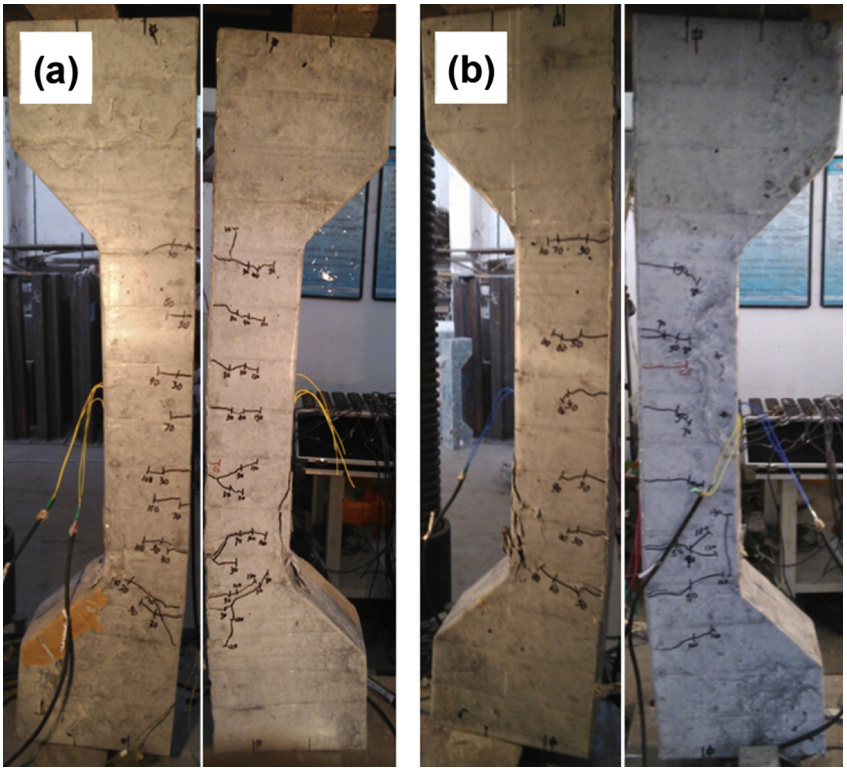

Fig. 5. Failure of ordinary plain concrete specimens under large eccentricity (e = 80 mm): (a) OPCC-LE1; (b) OPCC-LE2.

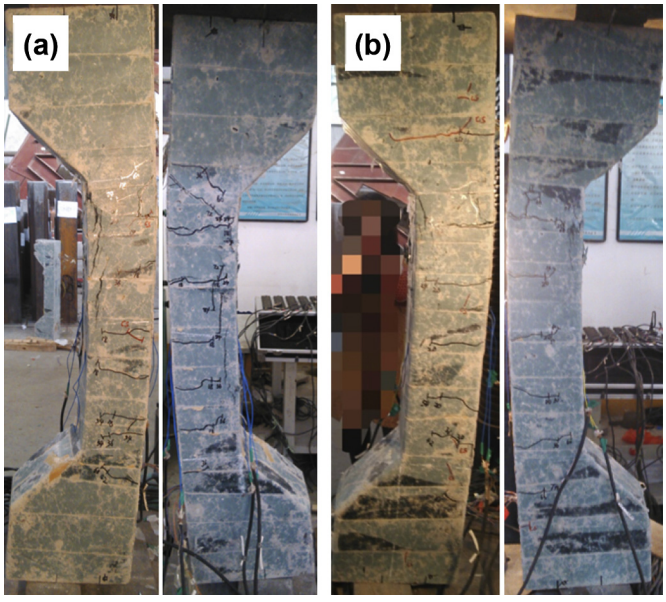

Fig. 6. Failure of inorganic polymer concrete specimens under large eccentricity (e = 80 mm): (a) IPCC-LE1; (b) IPCC-LE2.

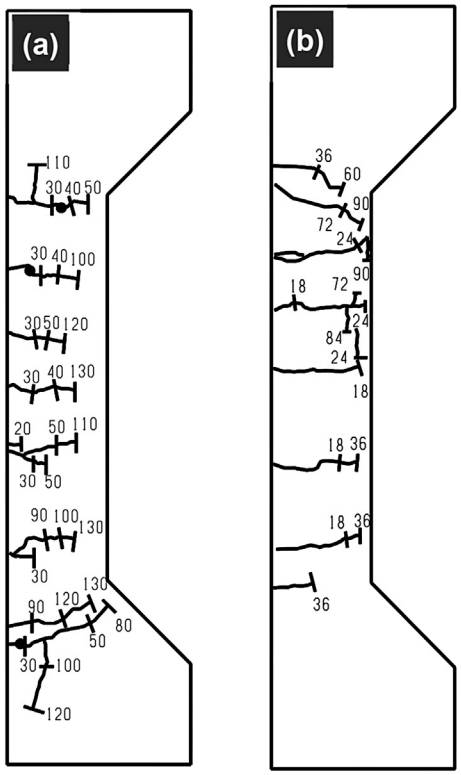

Fig. 7. Crack patterns of specimens under large eccentricity (e = 80 mm): (a) OPCC-LE1; (b) IPCC-LE1 (units in kN).

exhibited a bilinear behaviour starting from a linear elastic region, which was followed by another linear region with a smaller slope up to final failure. The yield point was evaluated from the change in the slope of load–displacement curve. The initial stiffness (defined as the slope of the first part of load–displacement curve) of OPCC equals to 16.1 kN/mm. The steel rebar on the tension face was yielded at a load of 120 kN and a lateral displacement of 7.3 mm. After the yield point, the stiffness of the specimen dropped sharply up to the failure of longitudinal steel rebars at a load of 130 kN and a lateral displacement of 10.1 mm.

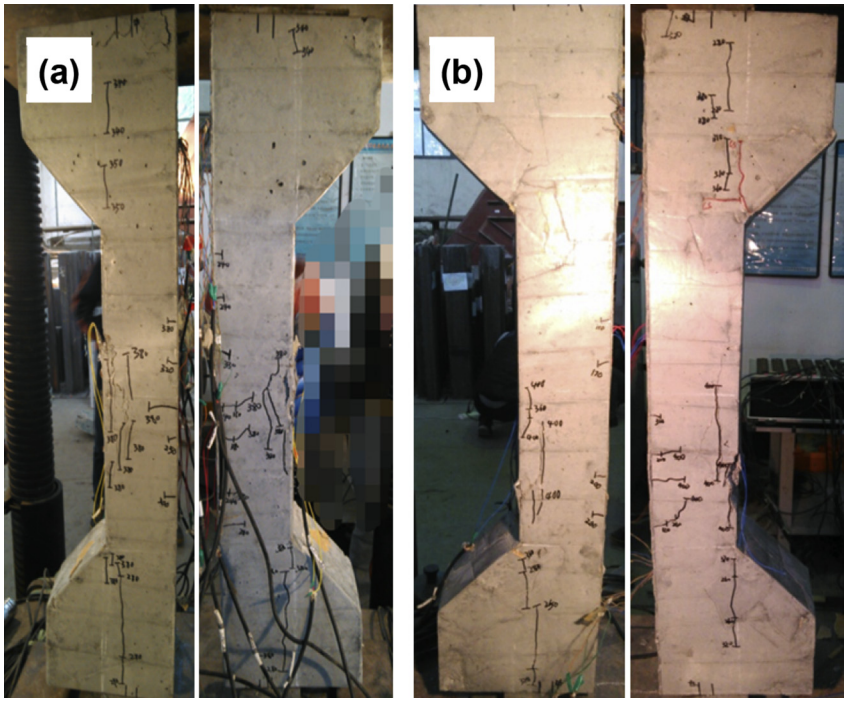

Fig. 8. Failure of ordinary plain concrete specimens under small eccentricity (e = 20 mm): (a) OPCC-SE1; (b) OPCC-SE2.

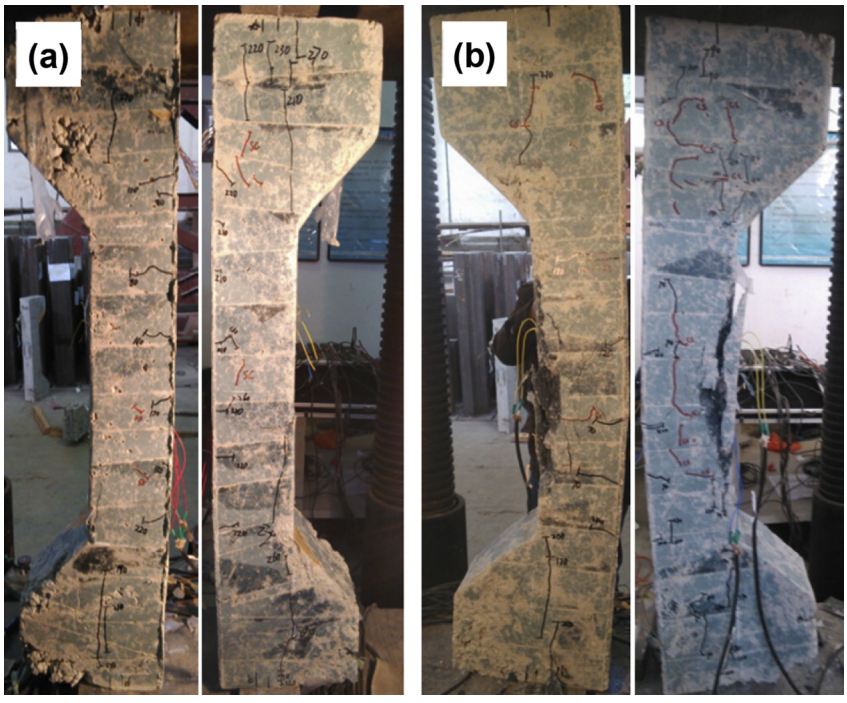

Fig. 9. Failure of inorganic polymer concrete specimens under small eccentricity (e = 20 mm): (a) IPCC-SE1; (b) IPCC-SE2.

The IPCC reinforced with basalt rebars had a nearly bilinear behaviour up to the failure. However, the yield point for IPCC was not obvious as compared to OPCC. This can be attributed to the fact that basalt rebar does not exhibit a clear yield point and the hardening region prior to ultimate failure is very small, as seen in Fig. 3. Initially, the concrete and basalt rebar work as a whole to carry the load. At a force of 18 kN and a lateral displacement of 1.6 mm, the first cracking on concrete occurred, and the load redistribution between concrete and basalt rebar happened. For IPCC, the initial stiffness was found to be 5.1 kN/mm, which is only about one third of that for OPCC. This can be associated with the much lower elastic modulus of basalt rebar in IPCC specimens than steel rebar in OPCC specimens. The failure load of IPCC was 90 kN, which is lower than that of OPCC, i.e., 130 kN, while the ultimate displacement of IPCC was approximately 65% larger than that of OPCC. This indicates that the IPCC specimens have better deformation capacity than control columns, i.e., OPCC.

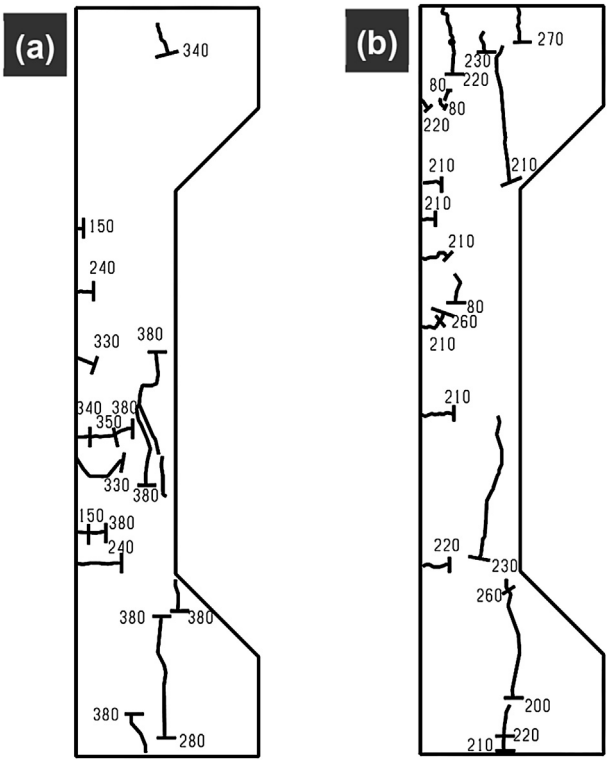

Fig. 10. Crack patterns of specimens under small eccentricity ($e = 20$ mm): (a) OPCC-SE1; (b) IPCC-SE1 (units in kN).

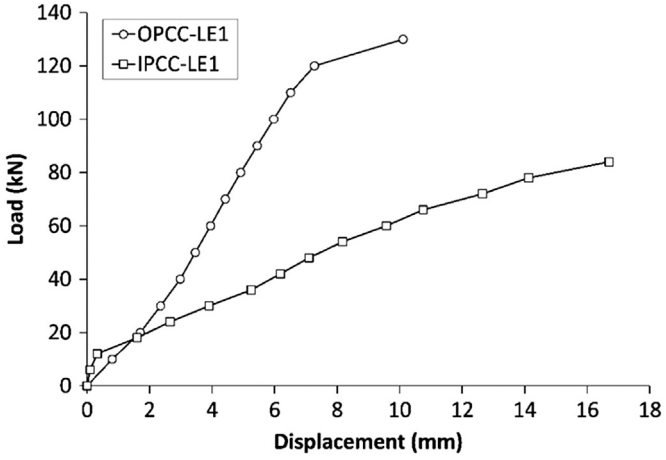

Fig. 11. Load–displacement behaviour of columns with large eccentricity.

In order to investigate the development of lateral displacements under loading along the column length, two additional displacement gages were placed at the upper and lower quantiles around the mid-height respectively to record the lateral displacement, as shown in Fig. 4. Fig. 12 shows the measured lateral displacements

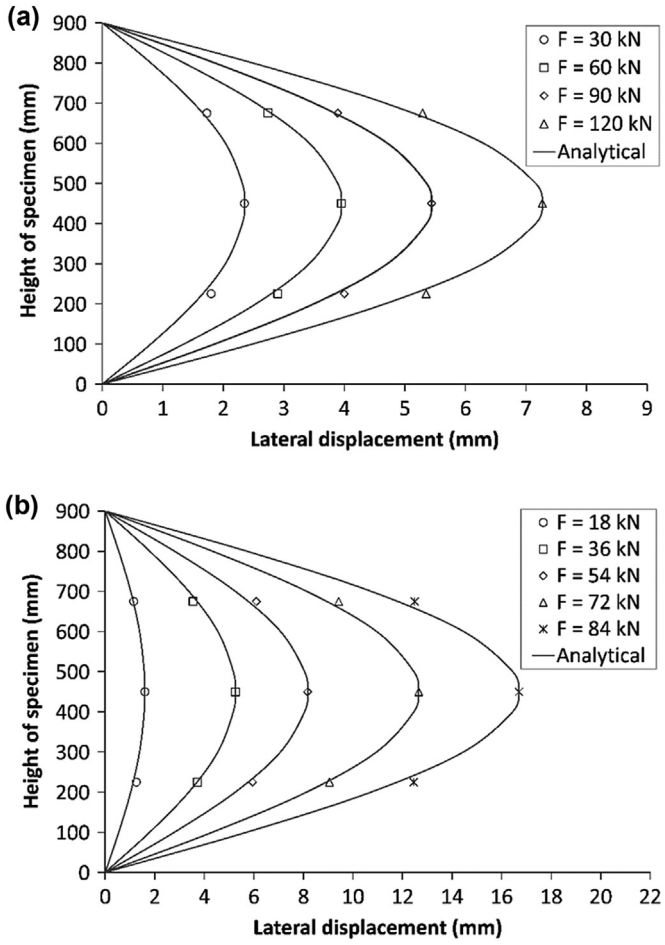

Fig. 12. Experimental and analytical lateral displacement of columns: (a) OPCC-LE1; (b) IPCC-LE1.

along the length of OPCC and IPCC at different stages of loading up to final failure. It can be observed that for both the specimens the lateral displacements at upper and lower quantiles are very close to each other during loading.

For ordinary reinforced concrete columns, the lateral displacement at a specific position along the column length, δ, can be described using the sine-shaped model, $\delta = \Delta \cdot \sin\left(\frac{\pi x}{L}\right)$, in which Δ denotes the maximum lateral displacement at the mid-height section, x represents the longitudinal coordinate variable and L is the column length. The analytical results obtained by this formula for the specimens of OPCC and IPCC are plotted together with experimental data in Fig. 12, which indicates that there is a very good agreement between the experimental data and analytical results. This implies that the sine-shaped model for ordinary reinforced concrete columns can be used for inorganic polymer concrete columns reinforced with basalt FRP bars to predict the lateral deformation along the column length at various load levels until final failure.

Table 7
Load and mid-height displacements of concrete column with large eccentricity.

Column	Cracking		Yielding		Failure	
	Load (kN)	Disp. (mm)	Load (kN)	Disp. (mm)	Load (kN)	Disp. (mm)
OPCC-LE1	20	1.7	120	6.0	130	10.1
IPCC-LE1	18	1.6	–	–	90	16.7

3.2.2. Small eccentricity

The load–displacement curves of the columns with small eccentricity (e = 20 mm) are shown in Fig. 13. Table 8 presents the values of loads and mid-height displacements corresponding to the first cracking, the yielding of reinforcement and the final failure of the column. As seen in Fig. 13, the overall behaviour of OPCC and IPCC are similar. It should be noted that the initial stiffness of IPCC is a little bit larger than OPCC before the initiation of cracks. The crack initiated at lateral displacements of 2.5 mm for OPCC and 1.7 mm for IPCC, respectively. After the crack initiation, the curves of the specimens were continued up to the yield point and the OPCC started to have a larger stiffness than IPCC. This can be attributed to the larger tensile and compressive strength of ordinary concrete in OPCC than inorganic polymer concrete in IPCC. Beyond the yield point, the slope of curves decreased. However, the decrease in the slope of curves up to final failure is less obvious than that for the specimens with small eccentricity shown in Fig. 11. This can be explained by the difference in failure modes between the specimens with large and small eccentricities, as shown in Figs. 7 and 10. The plastic region was continued until the concrete crushing and failure of longitudinal rebars on both tension and compression faces of the specimen at forces of 380 kN for OPCC and 270 kN for IPCC, respectively, and ultimate displacements of 5.4 mm for OPCC and 6.1 mm for IPCC, respectively. A nearly 15% larger ultimate displacement indicates that IPCC has a larger deformation capacity than OPCC under small eccentricity.

Compared to those with larger eccentricity, all specimens with small eccentricity exhibited a larger ultimate load, which can be ascribed to their different failure modes. For the specimen with small eccentricity, both the concrete and longitudinal rebars on the tension and compression faces made significant contribution to carrying the load, while for the specimen with large eccentricity only the concrete and longitudinal rebars on the tension face played a dominant role and the columns failed in tension-controlled failure. The difference in ultimate load between the specimens with large and small eccentricities is consistent with the difference in failure nodes of them as shown in Figs. 5–10.

3.3. Load–strain response of concrete

3.3.1. Large eccentricity

Fig. 14 shows the development of strain on the tension and compression faces at the mid-height section of the columns under large eccentricity with increasing load. At the early stage of loading, the longitudinal strain on the tension face of both OPCC and IPCC was small and the initial stiffness was large, as the concrete and reinforcement work together to resist tensile deformation. As load was increased, there was an obvious difference in the strain development of IPCC and OPCC that the longitudinal strain on the tension face of IPCC increased sharply due to crack initiation and quickly reached the maximum longitudinal strain of 2061 με due to crack growth up to tensile failure of inorganic polymer concrete on the tension face. Even though the load was slightly increased from to 18 kN–30 kN, while the tensile strain of OPCC showed a gradual increase with increasing load up to final failure after first cracking. This can be explained by the fact that the elastic modulus of steel rebar in OPCC is much larger than that of basalt rebar in IPCC.

On the compression face of the columns, OPCC and IPCC exhibited similar load–strain behaviour. The compressive strain increased gradually with increasing load, although the change in strain of OPCC with load level was less obvious than IPCC. The maximum longitudinal strain on the compression face of IPCC was equal to 3658 με, which is approximately 2 times that of OPCC. This can be ascribed to the larger deformation on the tension face of IPCC than OPCC, which results in a stress redistribution between the tension and compression faces of the specimen and a larger strain on the compression face of the specimen of IPCC. This result is consistent with that observed in the failure modes as shown in Figs. 5–10.

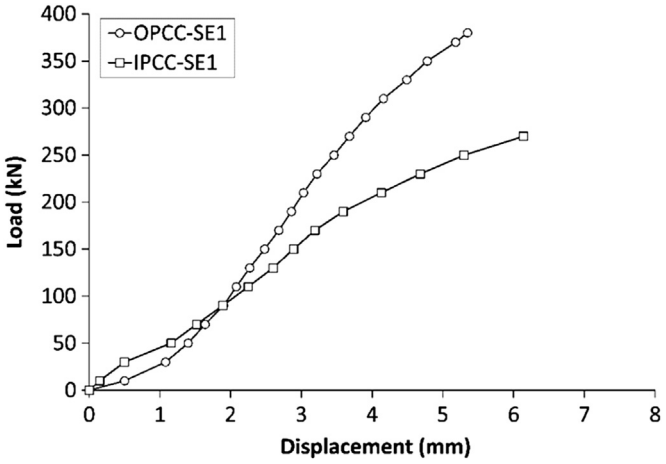

Fig. 13. Load–displacement behaviour of columns with small eccentricity.

3.3.2. Small eccentricity

Fig. 15 shows the development of strain on the tension and compression faces at the mid-height section of the columns under small eccentricity with increasing load. The overall behaviour of load–strain response for OPCC and IPCC under small eccentricity is almost similar to that under large eccentricity and the main different is the variation of longitudinal strain on the tension face of IPCC with load level that the longitudinal strain on the tension face increased slightly as load increased. This indicates that under small eccentricity the concrete on both tension and compression faces of the specimens contributed to bearing load and the specimens failed as a result of the crushing of concrete in the compression face before concrete on the tension face reached its ultimate tensile strain. The ultimate tensile strains of OPCC and IPCC were 1200 με and 195 με, respectively. The ultimate longitudinal strains on the compression faces of OPCC and IPCC were 2395 με and 2925 με, respectively, which show a 22% increase in ultimate compressive strain of IPCC beyond OPCC.

3.4. Load–strain response of reinforcement

In order to investigate the mechanical behaviour of longitudinal reinforcement in the columns under eccentric loading, the strain gauges were placed on the longitudinal reinforcement to record the change of strain with applied load. For each column, a total of 20 strain gauges were used, i.e. 5 strain gauges for each longitudinal reinforcement, the arrangement of which can be seen in Fig. 4. The strain gauges on each reinforcement along the length of column are labelled as I, II and III, respectively. For each column, the two reinforcements closer to the loading position are referred to as proximal reinforcement (PR), and the other two reinforcements are marked as distal reinforcement (DR). As the strain measured by the corresponding upper and lower strain gauges had a little difference, the average value of the corresponding strains is used in the analysis below.

3.4.1. Large eccentricity

Figs. 16 and 17 show the load–strain response of reinforcement in the specimens of OPCC and IPCC with large eccentricity. It can be observed that the strain at the mid-height section (i.e. III) was

Table 8
Load and mid-height displacements of concrete column with small eccentricity.

Column	Cracking		Yielding		Failure	
	Load (kN)	Disp. (mm)	Load (kN)	Disp. (mm)	Load (kN)	Disp. (mm)
OPCC-SE1	150	2.5	310	4.2	380	5.4
IPCC-SE1	80	1.7	–	–	270	6.1

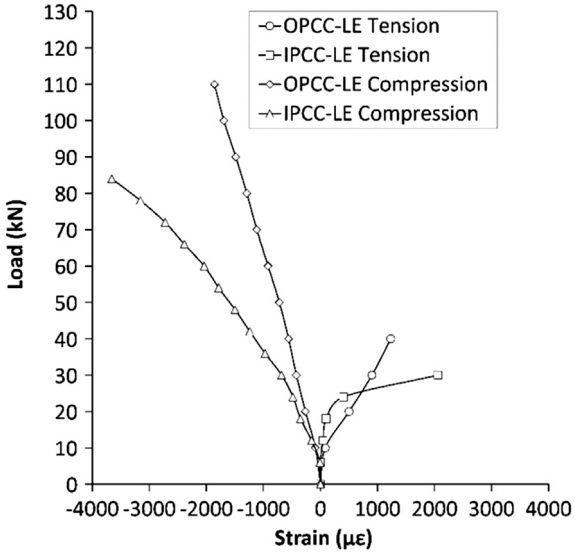

Fig. 14. Load–strain response of columns with large eccentricity.

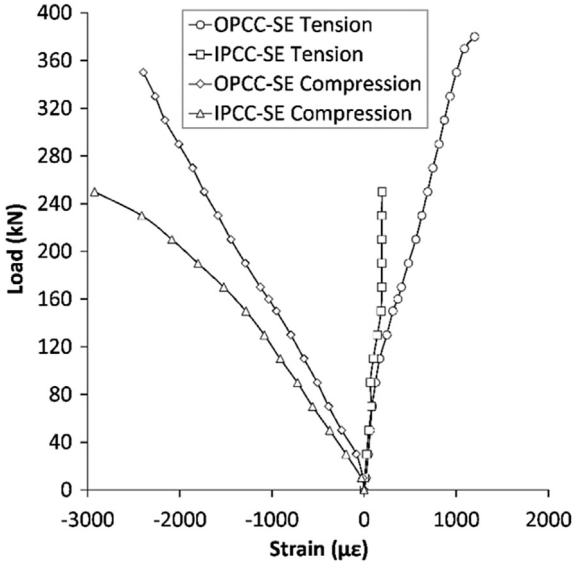

Fig. 15. Load–strain response of columns with small eccentricity.

largest and the strain at the section close to top and bottom surfaces (i.e. I) was smallest. The DR reinforcement was in tension, while the PR reinforcement was in compression.

As seen in Fig. 16, the load–strain response of the longitudinal reinforcement in OPCC exhibited a similar trend that the strain increased gradually with increasing load until the yield point. The steel rebars on the tension face of OPCC yielded at a force of approximately 110 kN and failed at a force of 120 kN. The average maximum longitudinal strains of steel rebars in OPCC with large eccentricity on the tension face were found to be 1506 με for DR I, 2841 με for DR II and 3734 με for DR III, respectively, which are much larger than the strain values of steel rebars on the compression face. This indicates that the columns under large eccentricity failed in tension-controlled failure.

As seen in Fig. 17, the overall load–strain behaviour of basalt rebars in IPCC was similar to that of steel rebars in OPCC. The strain on DR III was much larger than DR II and DR I. The DR reinforcement had a much larger longitudinal strain than PR reinforcement. However, no obvious yield point can be observed for basalt rebars in IPCC, which is very different to steel rebars in OPCC. This can be attributed to the fact that basalt rebar does not show a clear yield point, as seen in Fig. 3. The average maximum longitudinal strain of basalt rebar in IPCC on the tension face (DR III) was equal to 9817 με, which shows a 163% increase beyond DR III in OPCC. This can be ascribed to the smaller elastic modulus of basalt rebar in IPCC than steel rebar in OPCC. It should be noticed that the maximum strain of 9817 με of basalt rebar is a little bit smaller than the ultimate strain of basalt rebar obtained from the coupon test (see Fig. 3). Such difference seems logical, since the basalt rebar in the columns is not in a unidirectional stress condition that is different to the loading condition in the coupon tests. The ultimate load of basalt rebar in IPCC on the tension face was 90 kN, which is exactly the same as the load-bearing capacity of the specimen of IPCC, as shown in Fig. 11. This further indicates that the specimen with large eccentricity failed by the final failure of longitudinal basalt rebar and concrete crushing on the tension face. In addition, it can be noted that the maximum strains of PR reinforcements in IPCC and OPCC on the compression face were close to each other, the value of which was approximately 1500 με.

3.4.2. *Small eccentricity*

Figs. 18 and 19 show the load–strain response of reinforcement in the specimens of OPCC and IPCC with small eccentricity. It can be seen that the specimens with small eccentricity had different

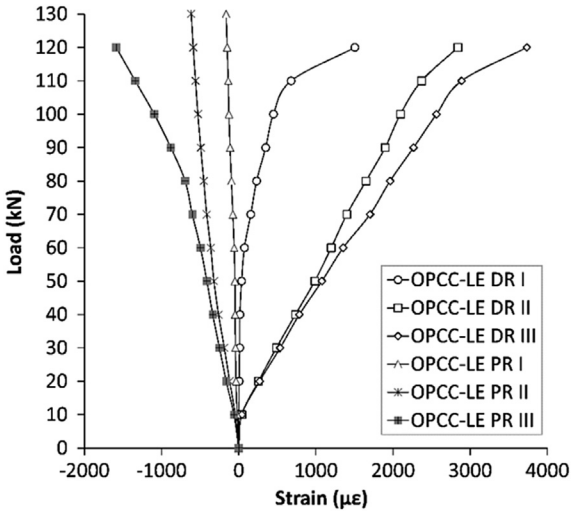

Fig. 16. Load–strain response of reinforcement in OPCC with large eccentricity.

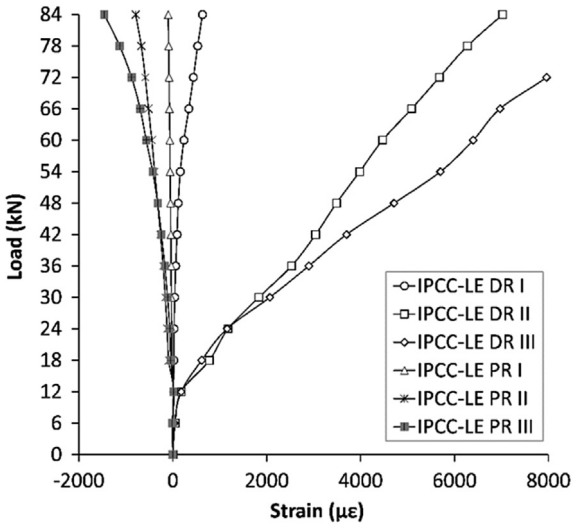

Fig. 17. Load–strain response of reinforcement in IPCC with large eccentricity.

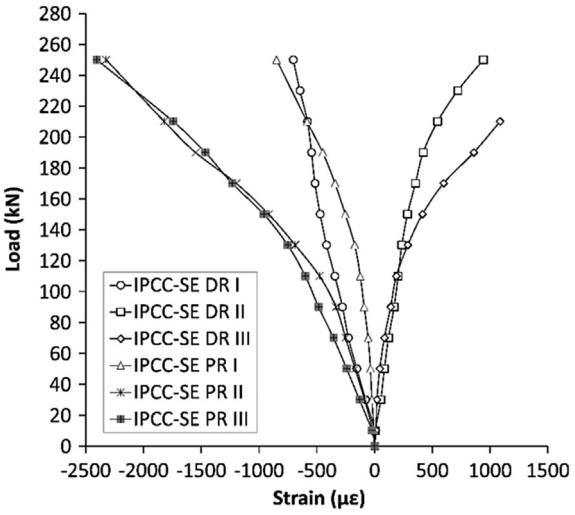

Fig. 19. Load–strain response of reinforcement in IPCC with small eccentricity.

behaviour with the specimens with large eccentricity. For the longitudinal reinforcements on the tension face of both OPCC and IPCC, DR II and DR III were in tension, while DR I was in compression. This indicates that some parts of the longitudinal reinforcement on the tension side would exhibit compressive behaviour under small eccentric loading, while all longitudinal reinforcement on the compression face of the columns was in compression.

As load increased, the longitudinal strain of basalt rebar in IPCC became larger than that of steel rebar in OPCC. This is due to smaller elastic modulus of basalt rebar than steel rebar, as a result of which the basalt rebar exhibited much larger deformation than steel rebar under the same load until the final failure of the specimen. The average maximum strains of the reinforcement on the tension face of IPCC and OPCC, i.e., IPCC-SE DR III and OPCC-SE DR III, were equal to 1087 με and 638 με, respectively, which indicates that the maximum strain of basalt rebar in IPCC was approximately 1.7 times that of steel rebar in OPCC.

It can be seen from Figs. 18 and 19 that the overall load–strain behaviour of reinforcement on the compression face of IPCC was similar with that of OPCC. The maximum longitudinal strains of the reinforcement on the compression face of IPCC and OPCC were found to be around 2500 με. Although there was initially a steady and almost linear increase in the compressive strain of all specimens with increasing load, however, the steel rebar in OPCC showed a clear yield point while the basalt rebar in IPCC did not. When the steel rebar in OPCC yielded, its compressive strain increased rapidly as load increased. However, for basalt rebar in IPCC, the rapid increase in compressive strain occurred when the load was approaching 1/4 of the maximum load.

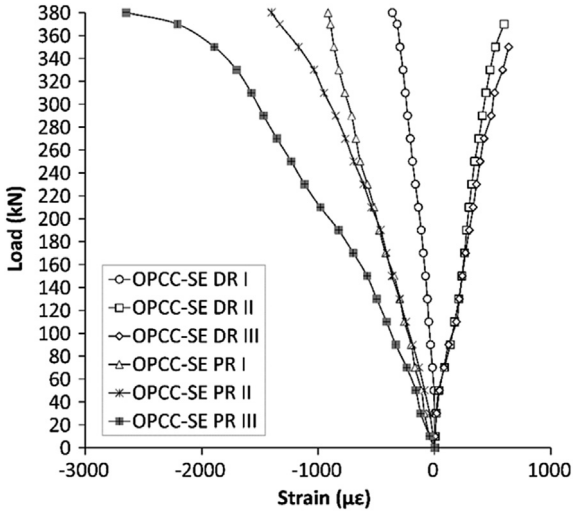

Fig. 18. Load–strain response of reinforcement in OPCC with small eccentricity.

3.5. Comparison with theoretical provisions

Herein, a theoretical prevision of the load-carrying capacity of the tested inorganic polymer concrete columns reinforced with basalt rebar is calculated and compared with the experimental results. Since performance of basalt rebar is different from steel rebar, the design provisions for steel reinforced concrete columns may not be applicable to basalt reinforced IPC columns. In this study, the load capacity of IPC columns is calculated according to the recommendations for concrete elements reinforced with FRP reinforcing bars presented in ACI 440.1R-15 [29] in conjunction with the following considerations and assumptions.

(1) The cross sections of short columns remain plane during the whole loading process.
(2) As seen in Table 6, the elastic moduli of inorganic polymer concrete and ordinary Portland cement concrete are close to each other. The strength development of inorganic polymer concrete is similar with ordinary Portland cement concrete, which can be described by the following equation.

$$\begin{cases} \sigma_c = f_c\left[1-\left(1-\dfrac{\varepsilon_c}{\varepsilon_0}\right)^n\right] & \varepsilon_c \le \varepsilon_0 \\ \sigma_c = f_c & \varepsilon_0 < \varepsilon_c \le \varepsilon_{cu} \end{cases} \quad (1)$$

with

$$\varepsilon_0 = 0.002 + 0.5\left(f_{cu,k} - 50\right) \times 10^{-5}$$

$$\varepsilon_{cu} = 0.0033 - \left(f_{cu,k} - 50\right) \times 10^{-5}$$

$$n = 2 - \frac{1}{60}\left(f_{cu,k} - 50\right)$$

where σ_c and ε_c denote the concrete stress and strain, respectively, ε_0 and ε_{cu} represent the concrete strain corresponding to the concrete stress of f_c and ultimate compressive strength $f_{cu,k}$, respectively.

(3) The stress–strain curve of basalt rebar is almost linear elastic, as can be seen in Fig. 4. For simplicity sake, it can be expressed by

$$\sigma_s = E_s\varepsilon_s \tag{2}$$

where σ_s, E_s and ε_s stand for the stress, elastic modulus and strain of basalt rebar, respectively.

(4) As the tensile strength of inorganic polymer concrete is much smaller than that of basalt rebar, therefore, it can be neglected and the basalt reinforcement is assumed to resist the tensile stress alone.
(5) The bonding between basalt rebar and inorganic polymer concrete is good and the debonding failure of reinforcing system would not occur before the ultimate load. In fact, this assumption can be verified using the measured load–strain response of basalt rebar at midspan, as shown in Figs. 17 and 19.

Fig. 20 shows a schematic diagram for calculating the load capacity of column subjected to eccentric compression. Based on the condition for equilibrium of forces and moments, and compatibility condition, the load capacity of columns can be obtained as follows:

$$\begin{cases} N = \alpha_1 f_c bx + \sigma'_s A'_s - \sigma_s A_s \\ Ne = \alpha_1 f_c bx\left(h_0 - \dfrac{x}{2}\right) + \sigma'_s A'_s (h_0 - a'_s) \end{cases} \tag{3}$$

with

$$x = \beta_1 x_0$$

$$\sigma_s = E_s\varepsilon_s = E_s\frac{h_0 - x_0}{x_0}\varepsilon_{cu} \quad \sigma'_s = E_s\varepsilon'_s = E_s\frac{x_0 - a'_s}{x_0}\varepsilon_{cu}$$

$$e = e_i + \frac{h}{2} - a_s$$

$$e_i = e_0 + e_a$$

where N is the ultimate load capacity, x is the balanced compression height, x_0 is the real balanced compressive height, α_1 and β_1 are the coefficients of equivalent rectangular stress and height of concrete (herein, α_1 and β_1 are taken as 1.0 and 0.8 respectively according to GB50010-2010 [30]), σ_s and σ'_s represent the stress of proximal and distal longitudinal basalt FRP bars, A_s and A'_s are the areas of proximal and distal longitudinal basalt FRP bars, a_s and a'_s stand for the distances from the outer surface of the concrete to the central axes of proximal and distal longitudinal basalt FRP bars, respectively, b and h_0 are the width and effective height of column's cross-section, ε_{cu} denotes the ultimate compressive strain ($\varepsilon_{cu} = 0.0035$), e_i, e_0 and e_a are eccentricity, initial eccentricity and additional eccentricity ($e_a = h/30 = 4$ mm), respectively.

The theoretical ultimate load capacity of the tested inorganic polymer concrete columns reinforced with basalt FRP bars with large eccentricity calculated using Eq. (3) equals 78.97 kN, which is about 88% of the measured load capacity of the tested beams. For the tested columns with small eccentricity, the predicted ultimate load capacity is equal to 210.7 kN, which is approximately 78% of the measured value. The generally good agreement between the theoretical prediction and experimental data confirms that the design codes for FRP-reinforced concrete column are applicable to inorganic polymer concrete column reinforced with basalt FRP bars.

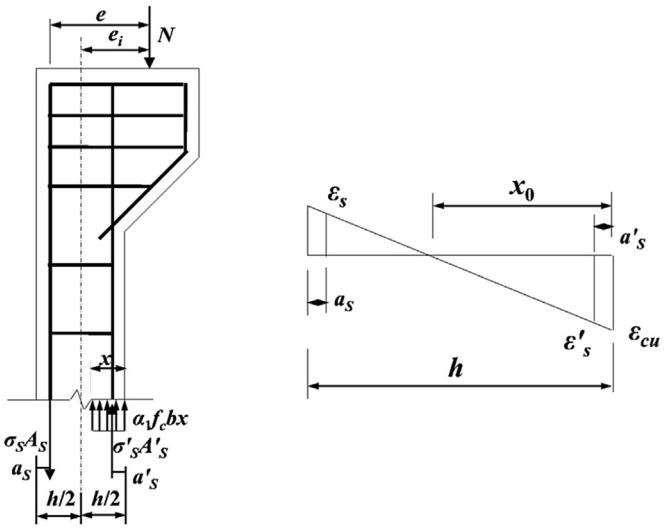

Fig. 20. Schematic diagram for calculating the load capacity of column subjected to eccentric compression.

4. Conclusions

An experimental study was carried out to investigate the mechanical behaviour of inorganic polymer concrete columns (IPCC) reinforced with basalt rebar under eccentric compression. The cracking patterns and development, and load–displacement/strain response of both concrete and reinforcement on the tension and compression faces of the specimens under large and small eccentricities were studied and compared with those of control steel-reinforced ordinary Portland cement concrete columns (OPCC), based on which the effect of eccentricity was addressed. The following main conclusions can be drawn from the present study:

- Under large eccentricity, the IPCC specimens had almost similar bilinear load–displacement response as the OPCC specimens up to the final failure as a result of concrete crushing and longitudinal reinforcement bulking on the tension face. However, the yield point for IPCC was not obvious as compared to OPCC, which can be attributed to the fact that basalt FRP bars in IPCC did not exhibit a clear yield point prior to ultimate failure. The load carrying capacity of IPCC with large eccentricity was around two thirds of that of OPCC, while the ultimate displacement of IPCC was approximately 65% larger than that of OPCC. This indicates that the IPCC specimens had better deformation capacity than OPCC.
- Under small eccentricity, the specimens were failed by the crushing of concrete and bulking of longitudinal reinforcement on both the tension and compression faces, which is different with the failure mode of specimens under large eccentricity. IPCC with small eccentricity was found to have about 30% lower load-carrying capacity than OPCC, while its ultimate displacement was approximately 15% larger than that of OPCC.
- The load–strain behaviour of concrete at the mid-height section on the tension and compression faces showed that the overall behaviour of load–strain response for all specimens under small eccentricity was almost similar to that under eccentricity. The maximum longitudinal strains on the compression face of IPCC under large and small eccentricities were approximately one

time and 22% respectively larger than those of OPCC, which can be ascribed to the larger deformation on the tension face of IPCC than OPCC due to the relatively lower strength of inorganic polymer concrete in IPCC than ordinary concrete in OPCC.
- The load–strain behaviour of longitudinal reinforcement of all specimens with small eccentricity was different to those with large eccentricity which leads to the different failure modes.
- The predicted lateral deformation along the column length under eccentric compression by using the sine-shaped model shows a good agreement with experimental data for all specimens at different load levels up to final failure indicates that this model can be used for design calculation of inorganic polymer columns reinforced with basalt FRP bars.

The inorganic polymer concrete reinforced with basalt FRP bar is a new composite system. In order to obtain a further understanding of the mechanical behaviour of this system under different loading conditions, it is vital to investigate the bond behaviour between inorganic polymer concrete and basalt FRP bar. This is the subject of ongoing research, the results of which will be presented in future publications.

Acknowledgements

The authors gratefully acknowledge the financial support from gs1:Wuhan University of Technology through grant number 631200321, the Fundamental Research Funds for the Central Universities (2012-04-070), China Scholarship (201206955021) and the National Key Technology Support Program (2014BAB15B01).

References

[1] Juenger MCG, Siddique R. Recent advances in understanding the role of supplementary cementitious materials in concrete. Cem Concr Res 2015;78:71–80.
[2] Sim K, Park C, Moon DY. Characteristics of basalt fiber as a strengthening material for concrete structures. Compos Part B 2005;36(6–7):504–12.
[3] Bakharev T. Resistance of geopolymer materials to acid attack. Cem Concr Res 2005;35(4):658–70.
[4] Duxson P, Fernández-Jiménez A, Provis JL, Lukey GC, Palomo A, Van Deventer JSJ. Geopolymer technology: the current state of the art. J Mater Sci 2007;42(9):2917–33.
[5] Sofi M, van Deventer JSJ, Mendis PA. Engineering properties of inorganic polymer concretes (IPCs). Cem Concr Res 2007;37:251–7.
[6] Hu SG, Wang HX, Zhang GZ, Ding QJ. Bonding and abrasion resistance of geopolymeric repair material made with steel slag. Cem Concr Comp 2008;30(3):239–44.
[7] Provis JL, Van Deventer JSJ. Geopolymers: structures, processing, properties, and industrial applications. Cambridge: Woodhead Publishing Limited; 2009.
[8] Herwig A, Motavalli M. Axial behavior of square reinforced concrete columns strengthened with lightweight concrete elements and unbonded GFRP wrapping. J Compos Constr 2012;16(6):747–52.
[9] Shi J, Zhu H, Wu Z, Wu G. Durability of BFRP and hybrid FRP sheets under freeze-thaw cycling. Adv Mater Res 2011;163–167:3297–300.
[10] Liu H, Lu Z, Peng Z. Test research on prestressed beam of inorganic polymer concrete. Mater Struct 2015;48:1919–30.
[11] Wei B, Cao H, Song S. Environmental resistance and mechanical performance of basalt and glass fibers. Mater Sci Eng A 2010;527(18–19):4708–15.
[12] Lee JJ, Song J, Kim H. Chemical stability of basalt fiber in alkaline solution. Fibres Polym 2014;15(11):2329–34.
[13] Li W, Xu J. Mechanical properties of basalt fiber reinforced geopolymeric concrete under impact loading. Mater Sci Eng A 2009;505:178–86.
[14] Wu G, Dong Z, Wang X, Zhu Y, Wu Z. Prediction of long-term performance and durability of BFRP bars under the combined effect of sustained load and corrosive solutions. J Compos Constr 2015;19(3):04014058.
[15] Tomlinson D, Fam A. Performance of concrete beams reinforced with basalt FRP for flexure and shear. J Compos Constr 2015;19(2):04014036.
[16] Zhang L, Sun Y, Xiong W. Experimental study on the flexural deflections of concrete beam reinforced with Basalt FRP bars. Mater Struct 2015;48:3279–93.
[17] Ge W, Zhang J, Cao D. Tu. Flexural behaviors of hybrid concrete beams reinforced with BFRP bars and steel bars. Constr Build Mater 2015;87:28–37.
[18] A. El Refai, F. Abed. Concrete contribution to shear strength of beams reinforced with basalt fiber-reinforced bars. J Compos Constr 10.1061/(ASCE)CC.1943-5614.0000648, 04015082.
[19] Sumajouw DMJ, Hardjito D, Wallah SE, Rangan BV. Fly ash-based geopolymer concrete study of slender reinforced columns. J Mater Sci 2007;42:3124–30.
[20] Sarker PK. Bond strength of reinforcing steel embedded in fly ash-based geopolymer concrete. Mater Struct 2011;44:1021–30.
[21] Gu X, Qiao D. Laboratory test and numerical simulation of bond performance between basalt fiber reinforced polymer rebar and concrete. J Test Eval 2012;40(7):1–8.
[22] Castel A, Foster SJ. Bond strength between blended slag and Class F fly ash geopolymer concrete with steel reinforcement. Cem Concr Res 2015;72:48–53.
[23] Ganesan N, Indira PV. Bond behaviour of reinforcing bars embedded in steel fibre reinforced geopolymer concrete. Mag Concr Res 2015;67(1):9–16.
[24] El Refai A, Ammar MA, Masmoudi R. Bond performance of basalt fiber-reinforced polymer bars to concrete. J Compos Constr 2015;19(3):04014050.
[25] Wang H, Sun X, Peng G, Luo Y, Ying Q. Experimental study on bond behaviour between BFRP bar and engineered cementitious composite. Constr Build Mater 2015;95:448–56.
[26] Fan X, Zhang M. Experimental study on flexural behaviour of inorganic polymer concrete beams reinforced with basalt rebar. Compos Part B 2016;93:174–83.
[27] Ministry of Construction of the People's Republic of China. Standard for test method of mechanical properties on ordinary concrete – GB/T 50081-2002. 2003. Beijing, China.
[28] Ministry of Housing and Urban-Rural Development of the People's Republic of China. Standard for test method of concrete structures – GB/T 50152-2012. 2012. Beijing, China.
[29] American Concrete Institute (ACI) Committee 440. Guide for the design and construction of structural concrete reinforced with fiber-reinforced polymer (FRP) bars – ACI 440.1R-15. Farmington Hills, MI: ACI; 2015.
[30] Ministry of Housing and Urban-Rural Development of the People's Republic of China. Code for design of concrete structures – GB 50010-2010. 2010. Beijing, China.